# Prediction and Comparison of Creep Behavior of X20 Steam Plant Piping Network with Different Phenomenological Creep Models

*Smith Salifu, Dawood Desai, and Schalk Kok*

Submitted: 25 March 2020 / Revised: 16 June 2020 / Accepted: 24 September 2020 / Published online: 28 October 2020

**In service, steam pipes are subjected to high temperature close to 0.4 $T_m$ (melting temperature) or higher and pressure; thus, making them prone to failure due to creep. Often, the design methods for these steam pipes usually do not provide their specific in-service life; hence, some type of service fitness tests are performed, and data obtained from the tests are used to inform the routine inspections. Choosing a creep model that favorably describe the creep behavior of components in service is paramount to engineers as well as the plant operators. Reports have shown that there are several creep models available and they all behave differently with different materials, and operating conditions. In this study, the creep behavior of X20 (12Cr-1MoVNi) steam piping network subjected to three phenomenological creep models (conventional hyperbolic sine creep, modified hyperbolic sine creep and constitutive creep model) was investigated. Fortran user subroutine scripts were developed for the three models and implemented in finite element (FE) code, Abaqus to determine the creep stress and strain rate, while the useful creep life and creep damage was determined using fe-safe/TURBOlife software. The results show that the modified hyperbolic sine creep model is more suitable for estimating the creep behavior of X20 steam piping under the specified operating conditions because of its more conservative prediction.**

**Keywords** Abaqus, creep rate, creep models, fe-safe/TURBOlife, intrados, loglife, X20

## 1. Introduction

Creep failure is a major concern for high-temperature components and structures in power generation plants (Ref 1, 2). The unplanned failure of these components represents the reality of the power generation plants as the increasing demand for energy has posed enormous pressure on the components in the form of an increase in operating conditions such as temperature and pressure. Hence, the determination of the useful creep life/behavior of power generation plant's components particularly, the steam pipes has been a foremost issue due to its direct link to safety and economy (Ref 3). X20 steel (12Cr-1MoVNi) is widely used for making components such as steam pipes and turbine blades that are subjected to operation in the creep regime due to its excellent corrosion and heat resistance (Ref 4, 5).

Over the years, the X20 piping systems have been inspected and re-inspected using the replica method, and the result of the inspection was used to study the service performance of the steel. As a complement to this inspection technique, finite element method (FEM) has been used successfully to gain a better understanding of the creep behavior of the steel (Ref 2), and several creep models have been employed and used to determine the creep behavior of this piping material. In addition, the creep behavior of high-temperature components has been studied by several authors over time (Ref 6-10). In their studies, different creep models were used to estimate the creep behavior of the components and the components were observed to behave differently. Sadly, reports have shown that there is no appropriate creep model, and the available ones behave differently with different materials and operating conditions. In the event of choosing a wrong model, wrong creep behavior is predicted and the consequence could be detrimental.

One of the most commonly used creep models for calculating creep rate based on its simplicity is the creep power-law model (Ref 11). Both the time and strain hardening version of the model are limited by relatively low stress or creep constants (Ref 11). Since high stresses are usually encountered during the operation of steam pipes and the creep rates often display exponential dependence on stress, a creep model that shows such dependence on stress at high-stress level should be adopted when creep rate is to be determined (Ref 11), and the model should be able to describe the inelastic behavior of the component at elevated temperature (Ref 12).

In this paper, the creep behavior of X20 steel (12Cr-1MoVNi) power generation steam piping network was computed using three different creep models, namely conventional hyperbolic sine creep, modified hyperbolic and constitutive creep models. The creep behavior of the piping network when subjected to a typical operating condition of 18 MPa and 550°C was simulated using Abaqus CAE/2019 in conjunction with fe-safe/TURBOlife software, and the most suitable of the three models with a more conservative creep rate and life prediction was determined.

**Smith Salifu** and **Dawood Desai**, Department of Mechanical and Automation Engineering, Tshwane University of Technology, Pretoria, South Africa; and **Schalk Kok**, Department of Mechanical and Aeronautical Engineering, University of Pretoria, Pretoria, South Africa. Contact e-mail: smithsalifu@gmail.com.

## 2. Mechanical and Thermal Stress Developed in a Straight Pipe

Three principal stresses namely hoop or circumferential stress $\sigma_t$, radial stress $\sigma_r$ and longitudinal or axial stress $\sigma_z$ are generated when a pipe or cylinder is subjected to internal pressure. Longitudinal stress occurs due to the thrust of pressure on the heads of the cylinder or pipe. The value of the hoop stress and radial stress varies throughout the cylinder, whereas the longitudinal stress is constant throughout (Ref 13). The circumferential, radial and axial stress for a thick wall cylinder with internal and external radius $r_i$ and $r_o$, subjected to internal pressure, $P$, was introduced by Lame (Ref 14). The generalized forms of these stresses are as follows:

$$\sigma_r = P\frac{r_i^2\left(r^2 - r_o^2\right)}{r^2\left(r_o^2 - r_i^2\right)}. \quad \text{(Eq 1)}$$

$$\sigma_t = P\frac{r_i^2\left(r^2 + r_o^2\right)}{r^2\left(r_o^2 - r_i^2\right)} \quad \text{(Eq 2)}$$

$$\sigma_z = \frac{P_i r_i^2}{r_o^2 - r_i^2} \quad \text{(Eq 3)}$$

Using the von Mises theory, the effective mechanical stress developed in the straight pipe or cylinder, $\sigma_m$ can be calculated.

$$\sigma_m = \sqrt{\left[\sigma_t^2 + \sigma_r^2 + \sigma_z^2 - (\sigma_t\sigma_r + \sigma_t\sigma_z + \sigma_r\sigma_z)\right]} \quad \text{(Eq 4)}$$

The thermal stress developed in straight thick pipe (Ref 15, 16) with internal and external radius $r_i$ and $r_o$ is given by:

$$\sigma_{tT} = \frac{\alpha E}{(1-\nu)r^2}\left[\frac{r^2 + r_i^2}{r_o^2 - r_i^2}\int_{r_i}^{r_o} Tr\mathrm{d}r - \int_{r_i}^{r} Tr\mathrm{d}r - Tr^2\right] \quad \text{(Eq 5)}$$

$$\sigma_{rT} = \frac{\alpha E}{(1-\nu)r^2}\left[\frac{r^2 - r_i^2}{r_o^2 - r_i^2}\int_{r_i}^{r_o} Tr\mathrm{d}r - \int_{r_i}^{r} Tr\mathrm{d}r\right] \quad \text{(Eq 6)}$$

$$\sigma_{zT} = \frac{\alpha E}{(1-\nu)}\left[\frac{2}{r_o^2 - r_i^2}\int_{r_i}^{r_o} Tr\mathrm{d}r - T\right] \quad \text{(Eq 7)}$$

The effective thermal stress is determined using von Mises theory.

$$\sigma_T = \sqrt{\left[\sigma_{tT}^2 + \sigma_{rT}^2 + \sigma_{zT}^2 - (\sigma_{tT}\sigma_{rT} + \sigma_{tT}\sigma_{zT} + \sigma_{rT}\sigma_{zT})\right]} \quad \text{(Eq 8)}$$

where $\sigma_r$, $\sigma_t$ and $\sigma_z$ is radial, circumferential and axial mechanical stress and $\sigma_{rT}$, $\sigma_{tT}$ and $\sigma_{zT}$ is thermal radial, circumferential and axial stress, respectively. $\sigma_m$ and $\sigma_T$ are effective mechanical and thermal von Mises stress.

Hence, the thermomechanical stress, $\sigma_{TM}$ developed in a straight pipe subjected to thermomechanical operation is obtained by the summation of the effective mechanical and thermal stresses obtained.

$$\sigma_{TM} = \sigma_m + \sigma_T \quad \text{(Eq 9)}$$

### 2.1 Hyperbolic Sine Creep Models

Hyperbolic sine creep model describes the relationship of creep strain rate, flow stress and temperature deformation. Also, the model has the ability to efficiently account for both high and low stress range (Ref 17) similar to that encountered in steam pipes. The conventional hyperbolic sine creep model equation (Ref 18-20) is given as:

$$\dot{\varepsilon}^{cr} = A\sinh(B\sigma)\exp\left(-\frac{Q}{RT}\right) \quad \text{(Eq 10)}$$

while the modified hyperbolic sine creep model equation (Ref 11, 21) developed by incorporating a stress exponent into the conventional hyperbolic sine creep model is given as:

$$\dot{\varepsilon}^{cr} = A\sinh(B\sigma)^n\exp\left(-\frac{Q}{RT}\right) \quad \text{(Eq 11)}$$

where $\dot{\varepsilon}^{cr}$ is minimum creep rate ($h^{-1}$), $Q$ is activation energy (J/(mol K), $R$ is gas constant equal to 8.314 J/(mol K), $T$ is absolute temperature in K and $A$, $B$ and $n$ are material constants, namely power-law multiplier ($h^{-1}$), hyperbolic multiplier (Pa) and stress exponent, respectively.

### 2.2 Constitutive Creep Model

As observed (Ref 12, 22, 23), a constitutive creep model formed by the summation of the linear and power-law stress functions (exponential) is given as:

$$\dot{\varepsilon}^{cr} = \varepsilon_p(T)\frac{\sigma}{\sigma_0(T)} + \varepsilon_p(T)\left(\frac{\sigma}{\sigma_0(T)}\right)^n \quad \text{(Eq 12)}$$

where $\sigma$ is the stress developed (Pa), $n$ is constant known as stress exponent and $\varepsilon_p(T)$, $\sigma_0(T)$ are Arrhenius functions of temperature.

### 2.3 Creep Damage

For materials that show limiting creep life prior to rupture, and defined as a function of stress and temperature, it is assumed that the cumulative damage is independent of the applied stress sequence. Thus, the linear damage rule suggested by Robinson is applicable (Ref 24, 25). The creep linear damage rule, also known as the time fracture rule is given as:

$$D_c = \sum\frac{t_i}{T_r} \quad \text{(Eq 13)}$$

where $D_c$ is creep damage, $t_i$ is creep duration under the applied temperature and stress increment i, and $T_r$ is creep life before rupture.

## 3. Material Properties

In order to simulate the creep behavior of X20 steel piping network, the following dimensions and material properties were used.

The creep material constants for the three models were obtained through curve fitting of experimental creep data of X20 steel at 550 °C. The constants are generated by determining the values of the best combination of each constant in the creep models that give the best fit with the experimental data of X20 steel obtained at 550 °C.

## 4. Analysis Methodology

### 4.1 Model Development

The pipe-insulation assembly model depicted in Fig. 1, 2 and 3 was developed in Abaqus CAE/2019 to mimic a real case scenario of a steam piping network used in typical power generation plants. Dimensions and material properties of the piping material, X20 steel and pyrogel insulation jacket are shown in Table 1, 2, 3 and 4. The constants for the creep analysis shown in Table 5, 6 and 7 were obtained through curve fitting of experimental data and were applied via the user Fortran subroutine scripts developed for the three models.

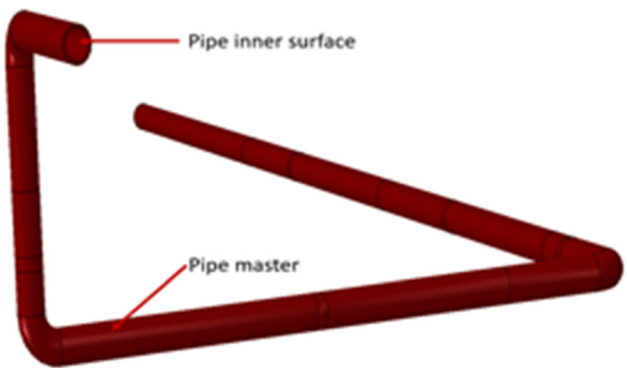


**Fig. 1** Model of piping network

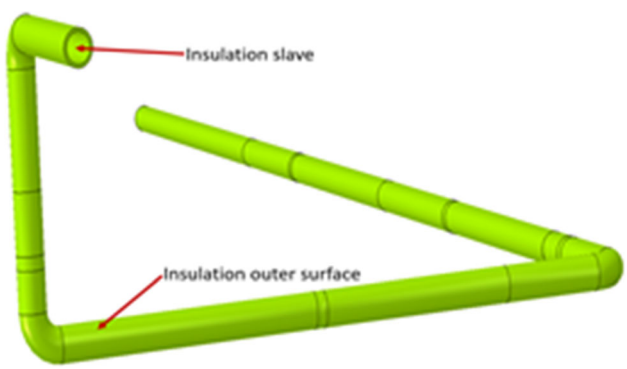


**Fig. 2** Model of insulation jacket

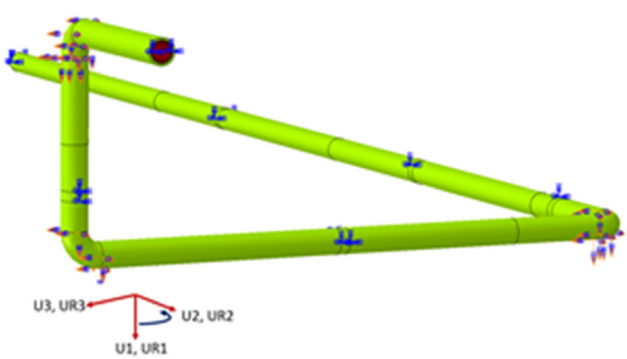


**Fig. 3** Model of pipe-insulation assembly

### 4.2 Interactions

In order to keep the pipe and insulation jacket together, tie interaction was created between the pipe master and insulation slave. Also, sink temperature of 550 °C representing the typical operating temperature of steam with film coefficient of 10000 W/($m^2$ K) representing the convective heat transfer coefficient of steam was applied to the pipe inner (Ref 29, 32). Similarly, 25 °C sink temperature and 18 W/($m^2$ K) film coefficient representing room temperature and convective heat transfer coefficient of air at room temperature, respectively, were applied to the outer surface of the insulation jacket (Ref 29, 33).

### 4.3 Analysis Steps

Three different steps, namely heat transfer, static general and viscoelastic steps in a sequentially coupled procedure were employed in this analysis. Heat transfer analysis was first carried out and the acquired nodal temperature distribution on the assembly was used as the driving operating temperature in the creep analysis consisting of static general and viscoelastic step (Ref 34).

### 4.4 Boundary Conditions/Loading

Displacement/Rotation boundary conditions were specified on the pipe-insulation assembly such that the assembly can be displaced in U1, U2 and U3 direction and rotate in the UR1, UR2 and UR3 direction at the elbows as shown in Fig. 3. An operating steam pressure of 18 MPa was applied to the pipe inner while the nodal temperature obtained from the heat transfer analysis was applied to the entire pipe-insulation assembly in step one of the predefined fields during the creep analysis.

### 4.5 Meshing

Hexagonal element shape was generated using sweep technique with advancing front algorithm, and the generated element shape was used throughout the analysis. Also, a mesh convergence study was conducted to determine the suitable mesh size for the analysis. This involves the reduction of the mesh size of the assembly until a suitable size that gives a high degree of accuracy will reasonable computational time was obtained (Ref 29). The study was conducted based on the thermomechanical stress developed in the pipe during operation, and a mesh size of 50 mm was found to be suitable for the analysis. 8-node linear heat transfer bricks element type, DC3D8 was assigned to the pipe-insulation assembly in the heat transfer analysis while an 8-node brick with a reduced integration hourglass control, C3D8R element type was assigned to the assembly in the creep analysis.

### 4.6 Creep Life

The output database file (ODB) from the creep analysis was exported and used in fe-safe/TURBOlife software to determine the useful life of the piping network under operational condition. In the analysis, two different surfaces, namely machine-finished $(16 < Ra \leq 40\ \mu m)$ and fine machine-finished $(4 < Ra \leq 16\ \mu m)$ were used and Morrow ductility exhaustion mean stress correction algorithm was applied (Ref 35). Also, the Neuber plasticity method and 0.33 follow-up factor were applied and the time, temperature and stress

**Table 1 Dimensions of steel pipe (Ref 26, 27)**

| Total length of pipe, m | External diameter, m | Internal diameter, m | Radius of elbow, m | Thickness of pipe, m |
|---|---|---|---|---|
| 52.1 | 0.44 | 0.38 | 0.50 | 0.03 |

**Table 2 Dimensions of pyrogel insulation jacket (Ref 28, 29)**

| Total length of insulation, m | External diameter of insulation, m | Internal diameter of insulation, m | Radius of elbow, m | Thickness of insulation, m |
|---|---|---|---|---|
| 52.10 | 0.54 | 0.44 | 0.50 | 0.05 |

**Table 3 Material constants for X20 steel (Ref 30)**

| Elasticity, GPa | Poisson ratio | Expansion, $\times 10^{-6}$ $K^{-1}$ | Density, kg/m$^3$ | Conductivity, W/mK | Specific heat capacity, J/kg K |
|---|---|---|---|---|---|
| 200 | 0.28 | 10 | 7 800 | 28 | 460 |

**Table 4 Material constants for pyrogel insulation jacket (Ref 29, 31)**

| Elasticity, MPa | Poisson ratio | Density, kg/m$^3$ | Expansion, $\times 10^{-6}$ $K^{-1}$ | Conductivity, $\times 10^{-6}$ W/mK | Specific heat capacity, J/kg K |
|---|---|---|---|---|---|
| 10 | 0.20 | 171 | 4.0 | 6.40 | 2 300 |

**Table 5 Modified hyperbolic sine creep constants for X20 steel at 550 °C (Ref 12)**

| $A$, $\times 10^{23}$ $h^{-1}$ | $B$, $\times 10^{-7}$ Pa | $n$ | $Q$, J/(molK) | $R$, J/mol | $T$, K |
|---|---|---|---|---|---|
| 1.059 | 2.490 | 0.672 | 530 811.1 | 8.314 | 823 |

**Table 6 Conventional hyperbolic sine creep constant for X20 steel at 550 °C (Ref 12)**

| $A$, $\times 10^{25}$ $h^{-1}$ | $B$, $\times 10^{-8}$ Pa | $Q$, J/(molK) | $R$, J/mol | $T$, K |
|---|---|---|---|---|
| 3.538 | 4.53 | 538 902.3 | 8.314 | 823 |

**Table 7 Constitutive creep equation constants for X20 steel (Ref 12)**

| | Material constants | | |
|---|---|---|---|
| Material | $\varepsilon_p(T)$, $\times 10^{-8}$ $h^{-1}$ | $\sigma_o(T)$, $\times 10^{8}$ Pa | $n$ |
| X20 | 8.752 | 1.255 | 10.678 |

increment from the imported ODB file was specified under the creep loading block of the software in order to determine the creep life and the damage of the pipe under the specified operating condition.

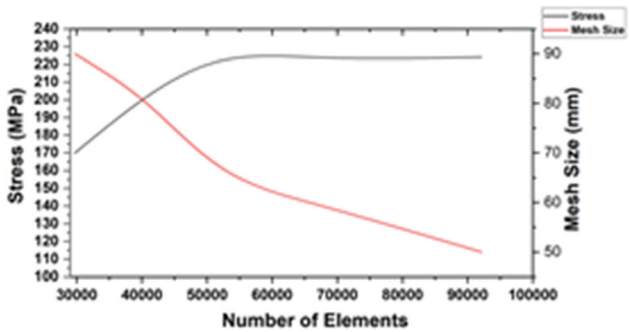


**Fig. 4** Mesh convergence study graph for X20 steel pipe

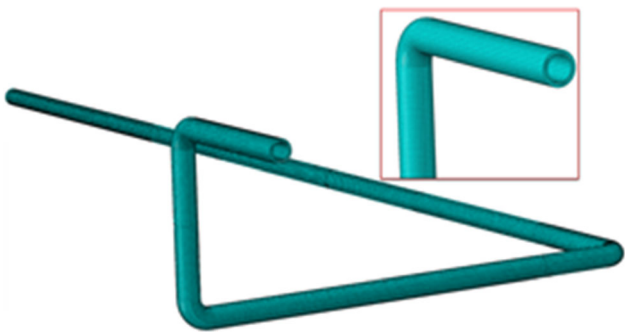

**Fig. 5** Pipe-insulation jacket assembly mesh

## 5. Results and Discussion

The mesh convergence study revealed a 50 mm mesh size with a total of 92126 elements and 155162 nodes to be suitable for the analysis. The graph of the mesh convergence study and the corresponding pipe-insulation assembly mesh is depicted in Fig. 4 and 5, respectively.

The result and temperature distribution profile contour obtained from the heat transfer analysis as indicated in Fig. 6 shows that the maximum operating temperature of 550 °C was maintained in the pipe while a minimum temperature of 39.93 °C was developed on the outer surface of the insulation jacket. This suggests that pyrogel is a good insulation jacket for steam pipes and the temperature of the outer surface can be reduced further by increasing the thickness of the jacket.

The creep stress and strain rates developed in the pipe-insulation assembly when subjected to operational condition using the different creep model specified is shown in Fig. 7, 8, 9, 10, 11 and 12. At operating pressure of 18 MPa and temperature of 550 °C, the predicted creep stress and strain rate for the conventional hyperbolic sine creep model are 222.3 MPa and $2.720 \times 10^{-5}$ $h^{-1}$, respectively. For the modified hyperbolic sine creep model, the creep stress is 222.1 MPa and the strain rate is $3.117 \times 10^{-5}$ $h^{-1}$ while the creep stress and strain for the constitutive creep model are 221.4 MPa and $4.131 \times 10^{-5}$ $h^{-1}$, respectively. In the three models, the maximum creep stress and strain rate were developed at the intrados of the elbow in the piping network. This is a pointer that creep failure will emanate from the intrados of the piping network regardless of the chosen creep model (Fig. 13).

Figure 14 is a plot of the logarithmic rate of the three models as a function of stress. The three models behave differently under different stresses. At the typical operating condition of the steam pipe, the constitutive creep model shows a higher creep rate while the conventional hyperbolic sine creep model gave the least creep rate. At a stress value lower than

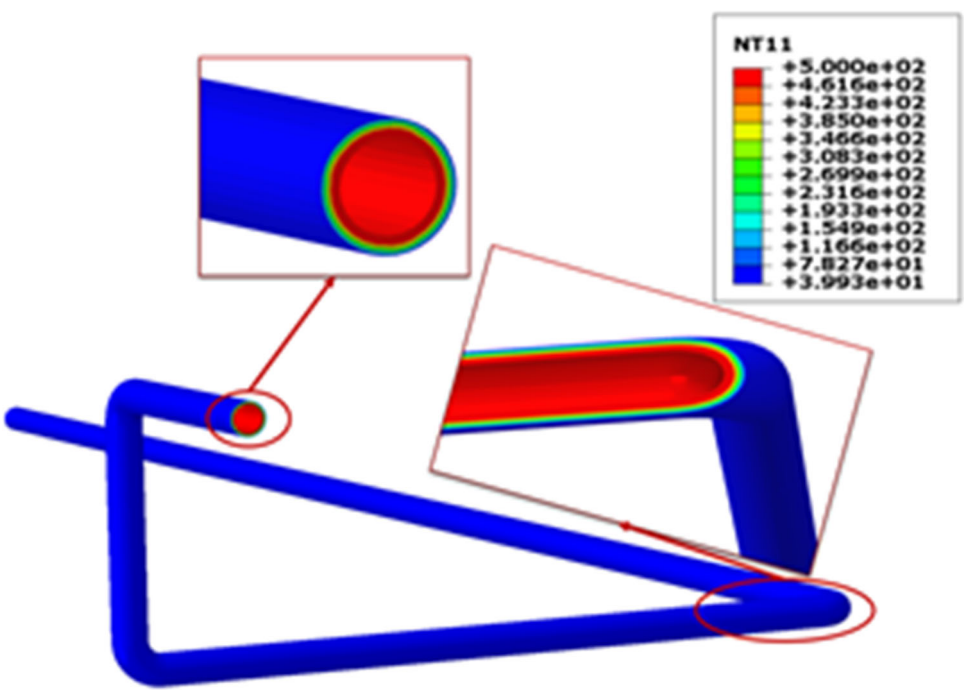


**Fig. 6** Temperature distribution profile of the pipe-insulation assembly

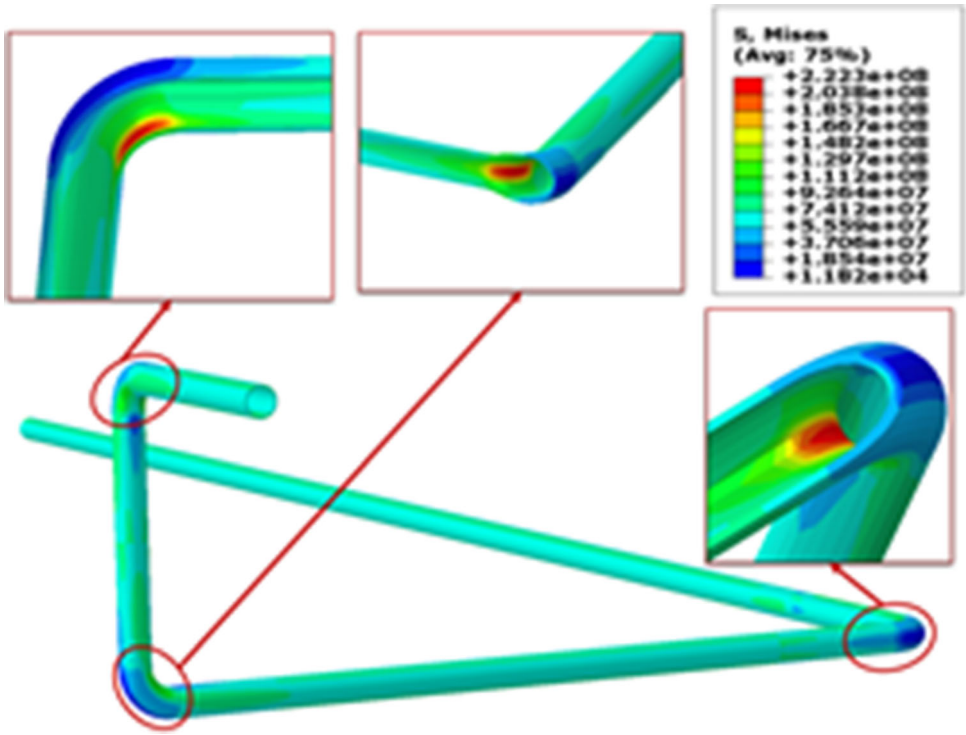


**Fig. 7** Creep stress developed under typical operating condition using conventional hyperbolic sine model

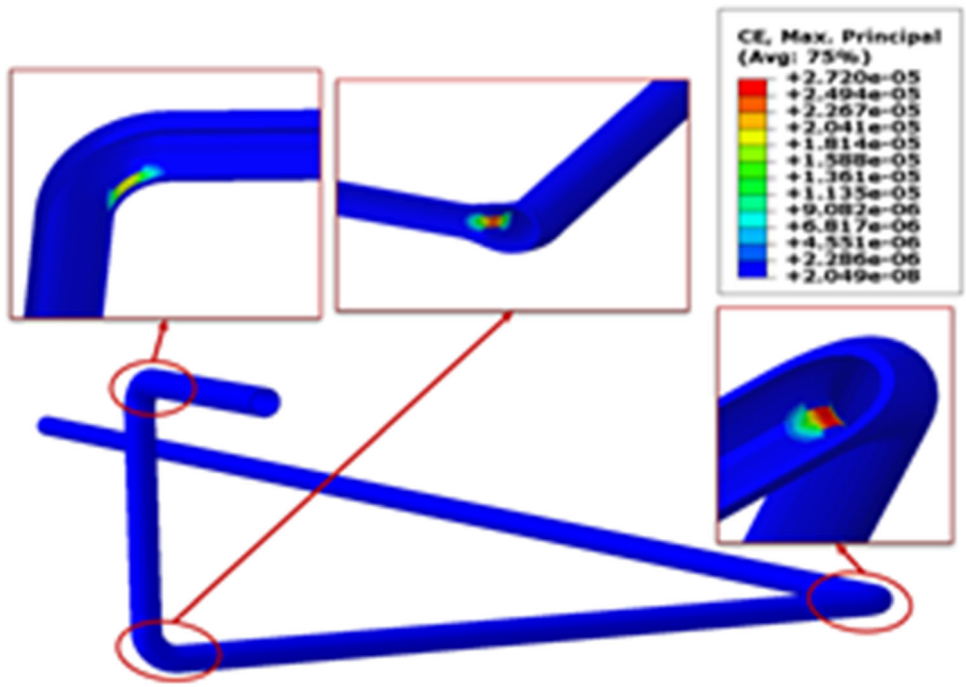


**Fig. 8** Creep rate developed under typical operating condition using conventional hyperbolic sine model

150 MPa, the constitutive creep model maintained its higher creep rate while the lowest rate was obtained using the modified hyperbolic sine creep model.

Under the typical operating condition of 18 MPa and 550 °C, the creep life of the X20 steam pipe subjected to the three creep models determined using fe-safe/TURBOlife show that the conventional hyperbolic sine creep model gave the highest creep life (19.66 and 21.95 years) while the modified hyperbolic sine creep model gave the least (15.26 and 16.85 years), depending on the surface finishing used. The contour plot, loglife and damage result for the three models under machine finished and fine machine-finished surfaces are shown

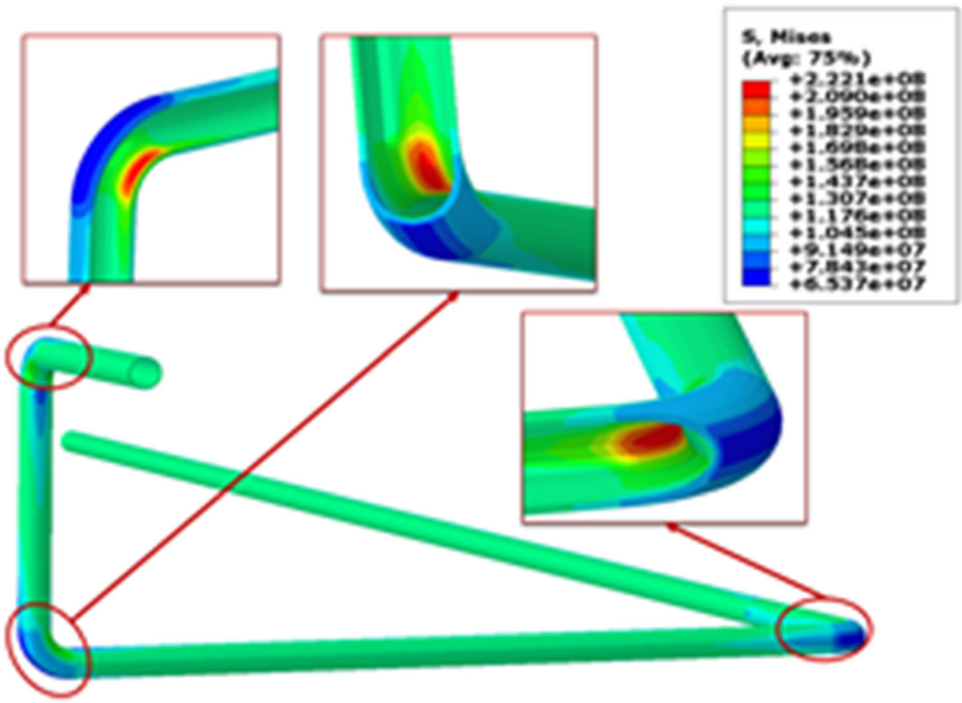


**Fig. 9** Creep stress developed under typical operating condition using modified hyperbolic sine model

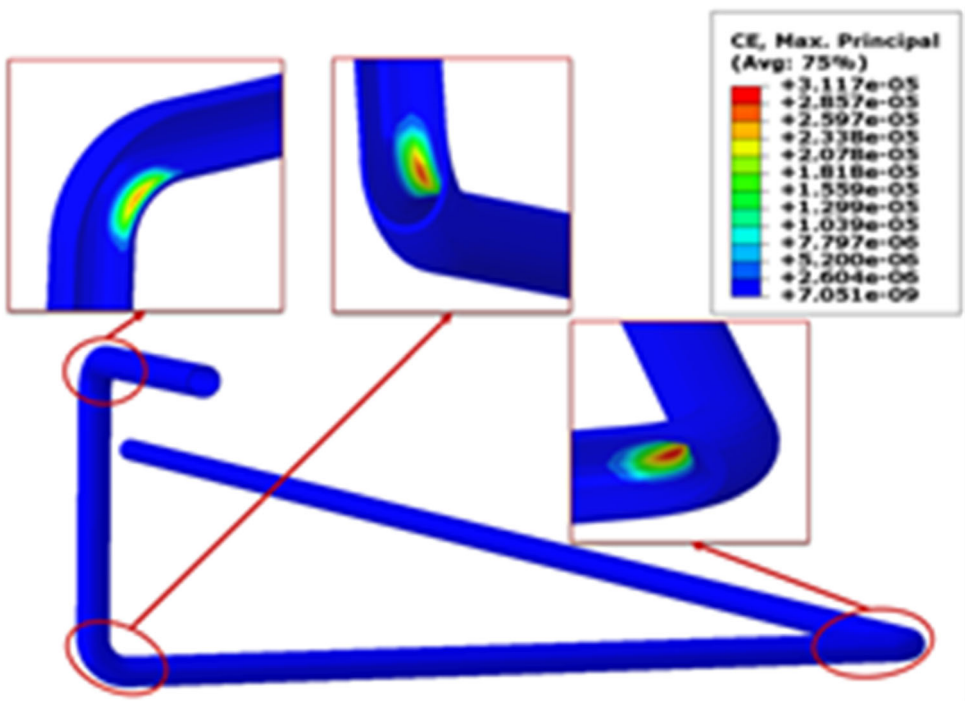


**Fig. 10** Creep rate developed under typical operating condition using modified hyperbolic sine model

in Fig. 15, 16, 17, 18, 19 and 20. Just like the maximum stress and strain rate result, the worst life and damage of the piping network for the three models considered are located at the intrados of the elbow and, the severity of damage and the useful life of the piping network is partly a function of the type of surface finish applied. The worst/useful life and damage of the piping network based on the three models and the surface finish used are shown in Table 8. Since the highest strain rate, worst life and damage is located at the intrados of the piping network elbow, failure of the piping network will emanate from this region regardless of the adopted model.

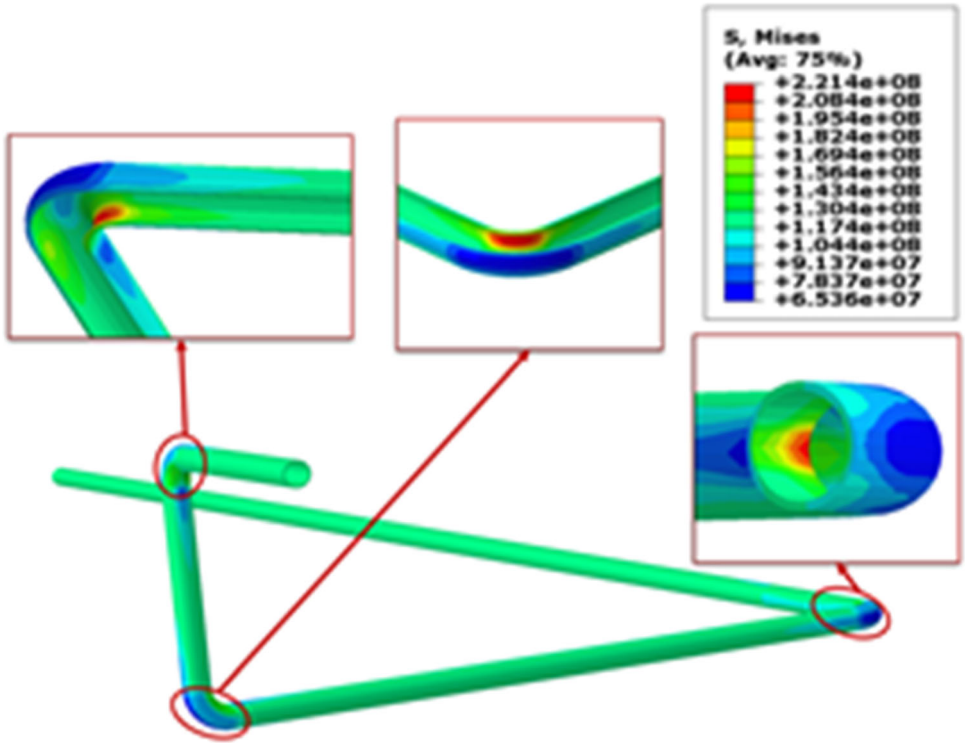


**Fig. 11** Creep stress developed under typical operating condition using constitutive creep model

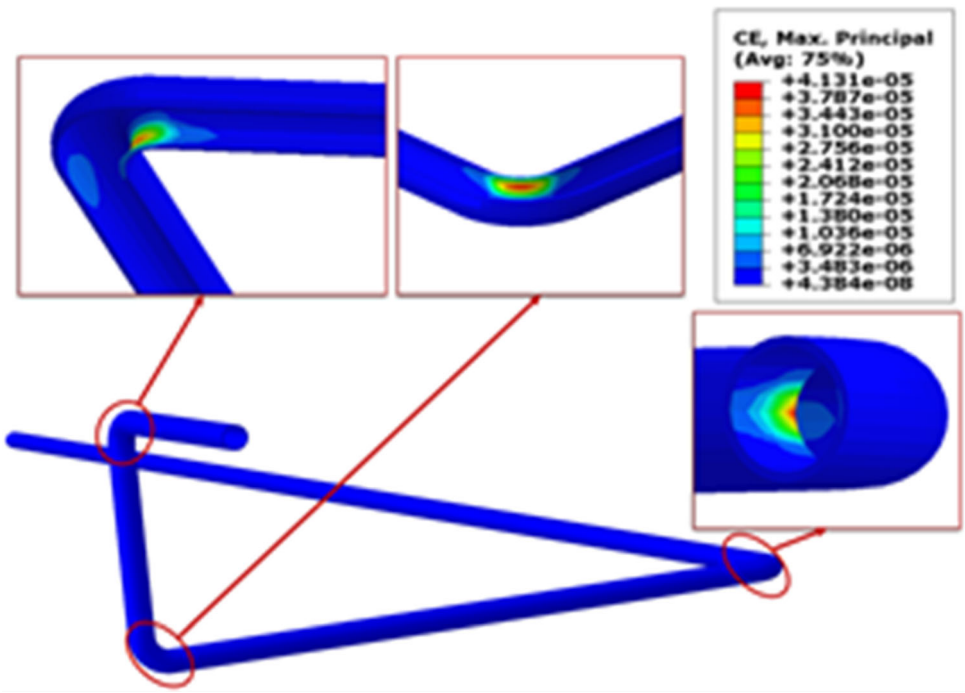


**Fig. 12** Creep rate developed under typical operating condition using constitutive creep model

### *5.1 Analytical Validation*

Due to the complexity of the piping network and the unavailability of established equation for the determination of thermomechanical stress in a complex piping network, only the strain rate at the straight region of the piping network can be validated analytically. Eq 1-9 was employed to determine the thermomechanical stress developed in the straight region of the

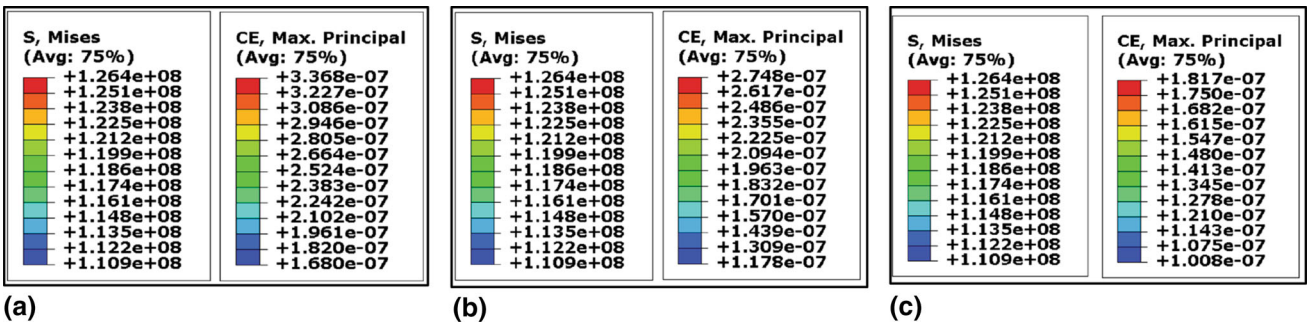


**Fig. 13** Stress and strain rate developed on the straight region of the piping network under a typical operating condition for (a) conventional hyperbolic sine creep model (b) modified hyperbolic sine creep model and (c) constitutive creep model

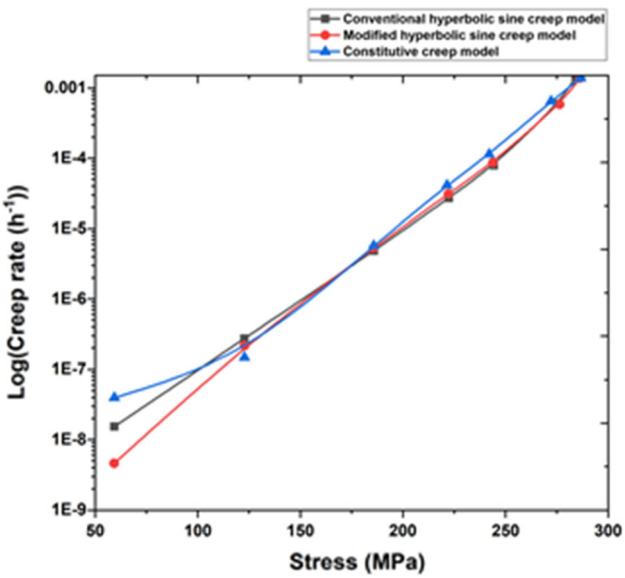


**Fig. 14** Comparison of the creep rate of the three creep models as a function of stress

piping network while the stress result obtained was used in conjunction with the three phenomenological creep model, Eq 10-12 to determine the strain rate at the straight region of the piping network when subjected to a typical operating condition of 18 MPa and 550 °C. A strong correlation was observed between the analytically calculated and numerically generated results since the % deviation between both is within the accepted range. The comparison of the analytically calculated and numerically simulated creep strain rate result for a straight region of the piping network is shown in Table 9, and the simulated results for the stress and strain rate at the region for the three models are shown in Fig. 13.

## 6. Conclusion

In this research, the creep behavior of X20 steam piping network under three different phenomenological creep models; conventional hyperbolic sine creep, modified hyperbolic sine creep and constitutive creep model was investigated using finite element code, Abaqus CAE/2019 in conjunction with fe-safe/TURBOlife software. The mesh convergence study conducted showed that 50 mm mesh size was suitable for the analysis and it generates highly accurate results with reasonable computational time.

The temperature distribution profile result and contour plot show that the maximum operating temperature (550 °C) was maintained in the pipe-insulation assembly while the value of temperature on the outer surface of the insulation jacket (39.93 °C) is an indication that pyrogel is a good insulation material suitable for use in power generation industry. The maximum creep stress of 222.3, 222.1 and 221.4 MPa, and strain rate $2.720 \times 10^{-5}$, $3.117 \times 10^{-5}$ and $4.131 \times 10^{-5}$ $h^{-1}$ for the conventional hyperbolic sine creep model, modified hyperbolic sine creep model and constitutive creep model, respectively, was developed at the intrados of the pipe's elbow.

Just like the creep stress and rate, the worst creep life and damage for the three models considered were found on the intrados of the pipe's elbow as expected with the modified hyperbolic sine model having the least creep life of 15.26 and 16.85 years for machine-finished and fine machine-finished surfaces, respectively, while the conventional hyperbolic sine creep model under the specified operating condition gave the highest creep life of 19.66 and 21.95 years for machine-finished and fine machine-finished surfaces, respectively. Hence, the modified hyperbolic sine creep model gave a more conservative creep behavior followed by the constitutive creep model by the virtue of their useful creep life prediction. Also, a strong correlation was observed between the numerically simulated and analytically computed creep rate for three models considered.

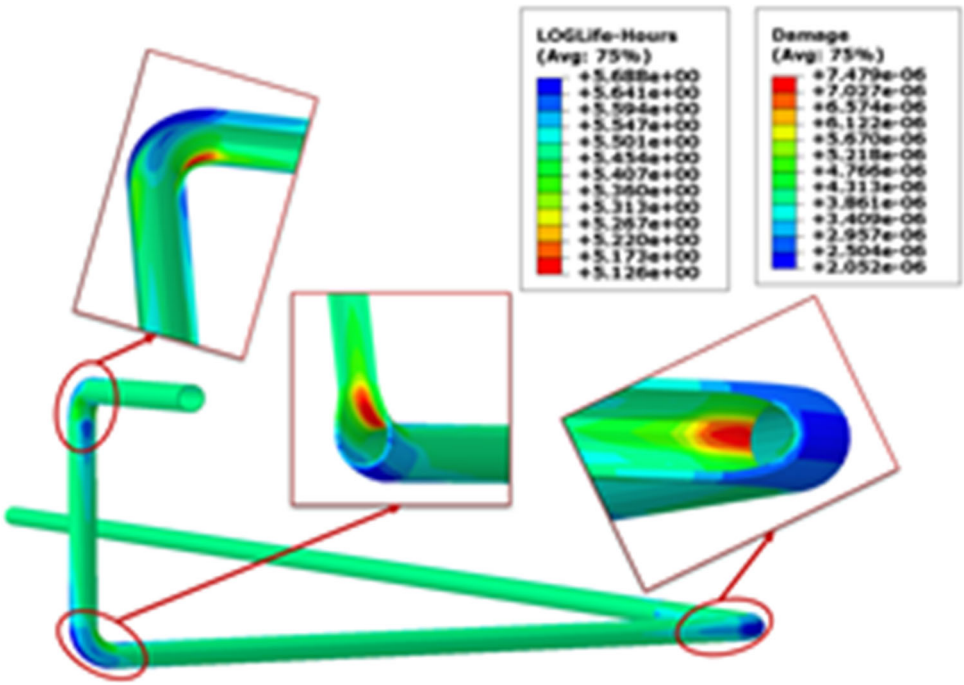


**Fig. 15** Creep loglife and damage of machined pipe under typical operating condition using modified hyperbolic sine model

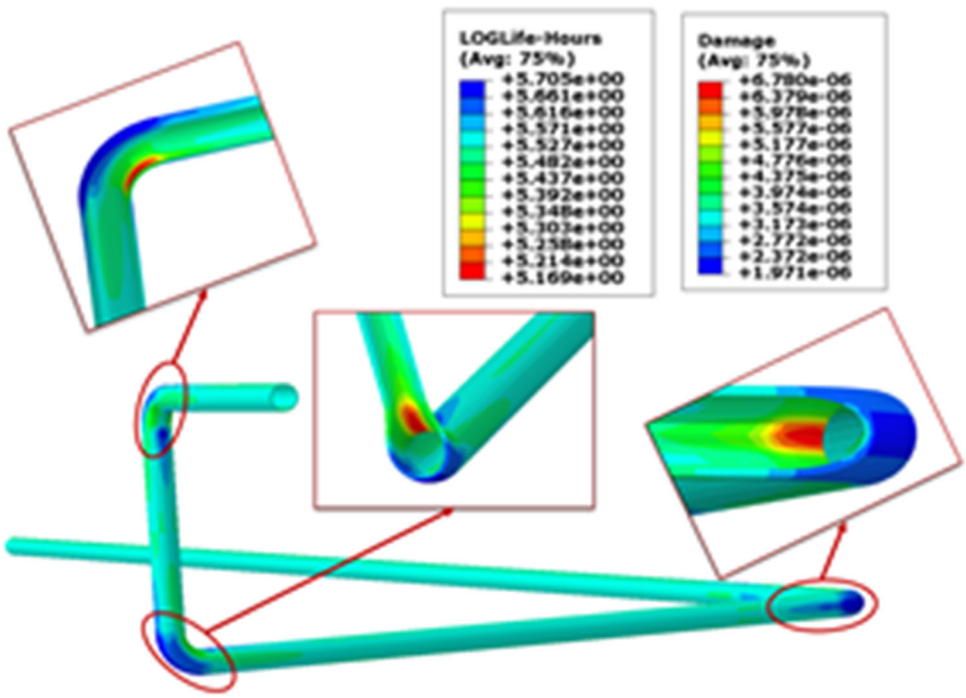


**Fig. 16** Creep loglife and damage of fine machined pipe under typical operating condition using modified hyperbolic sine model

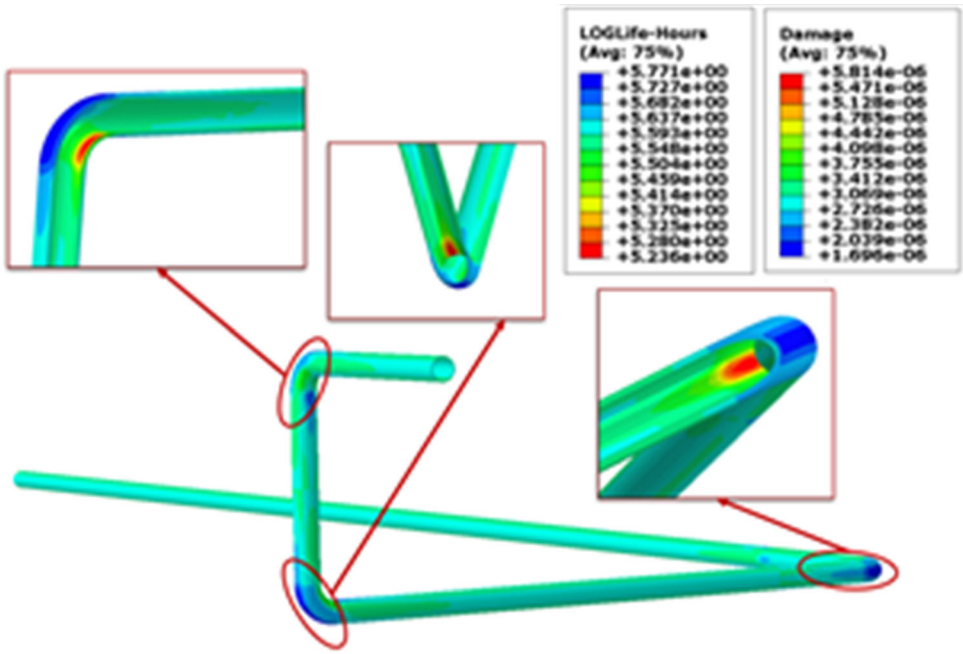


**Fig. 17** Creep loglife and damage of machined pipe under typical operating condition using conventional hyperbolic sine model

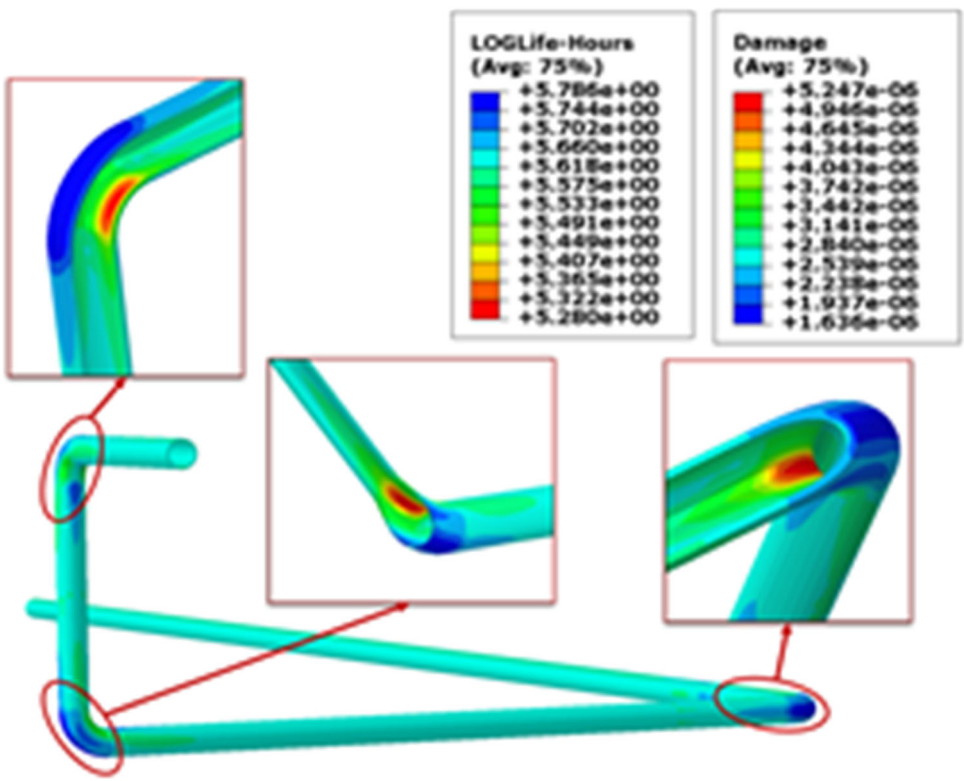


**Fig. 18** Creep loglife and damage of fine machined pipe under typical operating condition using conventional hyperbolic sine model

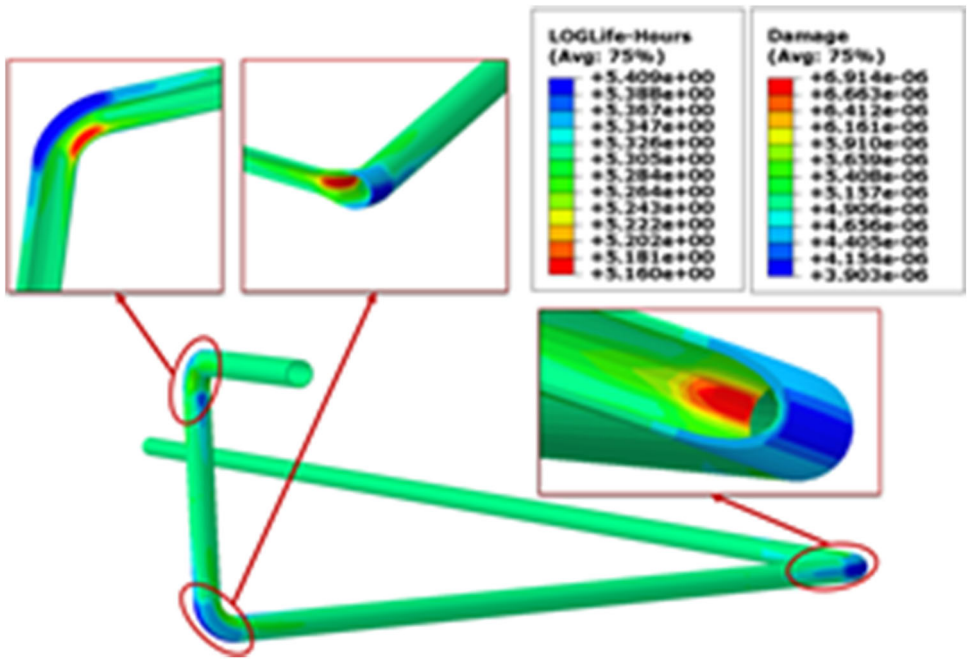


**Fig. 19** Creep loglife and damage of machined pipe under typical operating condition using constitutive model

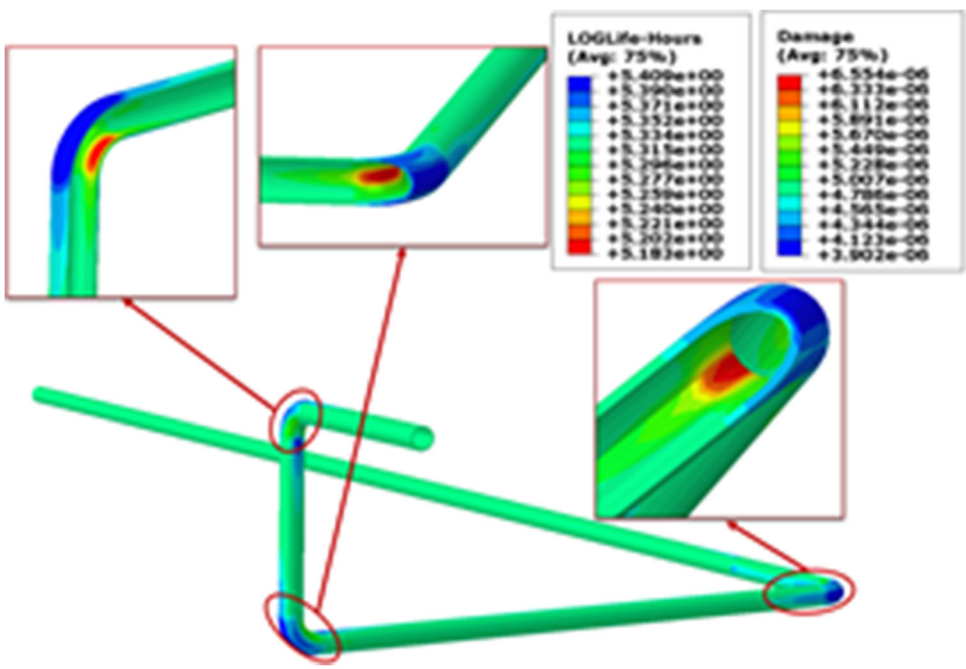


**Fig. 20** Creep loglife and damage of fine machined pipe under typical operating condition using constitutive model

Finally, the results obtained show that the modified hyperbolic sine creep model is more suitable for the prediction of the creep behavior of X20 steam pipes subjected to a typical operating condition of 18 MPa and 550 °C as it proffers a more conservative creep rate which will abet timely replacement and avert unforeseen catastrophe that is imminent when a less conservative model is selected.

**Table 8 Worst creep life and damage of X20 steam piping in operation under different creep models and surface finishing**

| Models | Machined finish | | | Fine machined finish | | |
|---|---|---|---|---|---|---|
| | Loglife | Life, years | Damage, $\times 10^{-6}$ | Loglife | Life, years | Damage, $\times 10^{-6}$ |
| Modified sine creep | 5.126 | 15.26 | 7.479 | 5.169 | 16.85 | 6.780 |
| Conventional sine creep | 5.236 | 19.66 | 5.814 | 5.284 | 21.75 | 5.247 |
| Constitutive creep | 5.160 | 16.5 | 6.914 | 5.183 | 17.40 | 6.554 |

**Table 9 Comparison of simulated and analytical creep rate of a straight region of the piping network for the three creep models under typical operating condition**

| Creep models | Analytical creep rate, $h^{-1}$ | Simulated creep rate, $h^{-1}$ | Deviation, % |
|---|---|---|---|
| Conventional hyperbolic sine | $3.450 \times 10^{-7}$ | $3.368 \times 10^{-7}$ | 2.38 |
| Modified hyperbolic sine | $2.820 \times 10^{-7}$ | $2.748 \times 10^{-7}$ | 2.55 |
| Constitutive creep | $1.860 \times 10^{-7}$ | $1.817 \times 10^{-7}$ | 2.31 |

## Acknowledgments

This work has been supported by Tshwane University of Technology and the University of Pretoria, South Africa. Also, the authors greatly appreciate the support of Eskom Power Plant Engineering Institute (Republic of South Africa).

## References

1. P. Auerkari, J. Salonen, S. Holmström, A. Laukkanen, J. Rantala, and R. Nikkarila, Creep damage and Long Term Life Modelling of an X20 Steam Line Component, *Eng. Fail. Anal.*, 2013, **35**, p 508–515
2. J. Storesund, K. Borggreen, and W. Zang, Creep Behaviour and Lifetime of Large Welds in X20 CrMOV 12 1—Results Based on Simulation and Inspection, *Int. J. Press. Vessel.*, 2006, **83**(11–12), p 875–883
3. S. Holmström, R. Pohja, A. Nurmela, P. Moilanen, and P. Auerkari, Creep and Creep-Fatigue Behaviour of 316 Stainless Steel, *Procedia Eng.*, 2013, **55**, p 160–164
4. D. Liu, D. Pons, and E. Wong, The Unified Creep-Fatigue Equation for Stainless Steel 316, *Metals*, 2016, **6**(9), p 219
5. S. Brett, S. Holmström, J. Hald, U. Borg, J. Aakjær, and R. van Vulpen, Creep Damage Development in Welded X20 and P91, *Int. J. Press. Vessel. Pip.*, 2011, **35**, p 508–515
6. P. Auerkari, S. Holmström, J. Veivo, and J. Salonen, Creep Damage and Expected Creep Life for Welded 9–11% Cr Steels, *Int. J. Press. Vessel.*, 2007, **84**(1–2), p 69–74
7. M. Yaguchi, T. Ogata, and T. Sakai, Creep Strength of High Chromium Steels Welded Parts under Multiaxial Stress Conditions, *Int. J. Press. Vessel.*, 2010, **87**(6), p 357–364
8. V. Gaffard, A.-F. Gourgues-Lorenzon, and J. Besson, High Temperature Creep Flow and Damage Properties of 9Cr1MoNbV Steels: Base Metal and Weldment, *Nuclear Eng.*, 2005, **235**(24), p 2547–2562
9. A. Yaghi, T. Hyde, A. Becker, and W. Sun, Finite Element Simulation of Welding Residual Stresses in Martensitic Steel Pipes, *Mater. Res. Innov.*, 2013, **17**(5), p 306–311
10. A. Yaghi, T. Hyde, A. Becker, and W. Sun, Finite Element Simulation of Welding and Residual Stresses in a P91 Steel Pipe Incorporating Solid-State Phase Transformation and Post-weld Heat Treatment, *J. Strain Anal. Eng. Des.*, 2008, **43**(5), p 275–293
11. F.Q. Yang, H. Xue, L.Y. Zhao and J. Tian, Calculations and Modeling of Material Constants in Hyperbolic-Sine Creep Model for 316 Stainless Steels, in *Applied Mechanics and Materials*, 2014, Trans Tech Publ
12. K. Naumenko, H. Altenbach, and A. Kutschke, A Constitutive Model for Creep and Long-Term Strength in Advanced Heat Resistant Steels and Structures, *J. Transit.*, 2009, **2**(3), p 4
13. D. Annaratone, Cylinders under Internal Pressure, *Press. Vessel. Des.*, 2007, **1**, p 47–125
14. B. Kanlıkama, A. Abuşoğlu, and İ.H. Güzelbey, Coupled Thermoelastic Analysis of Thick-Walled Pressurized Cylinders, *Int. J. Energy Power Eng.*, 2013, **2**(2), p 60–68
15. A. Kandil, A. El-Kady, and A. El-Kafrawy, Transient Thermal Stress Analysis of Thick-Walled Cylinders, *Int. J. Mech. Sci.*, 1995, **37**(7), p 721–732
16. V. Pesonen, Online Creep and Fatigue Monitoring in Power Plants, Master's thesis, 2014
17. J. Montes, F. Cuevas, and J. Cintas, New Creep Law, *Mater. Sci. Technol.*, 2012, **28**(3), p 377–379
18. B. Dyson, Use of CDM in Materials Modeling and Component Creep Life Prediction, *J. Press. Vessel. Technol.*, 2000, **122**(3), p 281–296
19. Q. Xu, Z. Lu, and X. Wang, Damage Modelling: The Current State and the Latest Progress on the Development of Creep Damage Constitutive Equations for High Cr Steels, *Mater. High Temp.*, 2017, **34**(3), p 229–237
20. Q. Xu, X. Yang, and Z. Lu, On the Development of Creep Damage Constitutive Equations: A Modified Hyperbolic Sine Law for Minimum Creep Strain Rate and Stress and Creep Fracture Criteria Based on Cavity Area Fraction along Grain Boundaries, *Mater. High Temp.*, 2017, **34**(5–6), p 323–332
21. Q. Xu, *Development of Advanced Creep Damage Constitutive Equations for Low Cr Alloy under Long-Term Service*, University of Huddersfield, Huddersfield, 2016
22. H.J. Frost and M.F. Ashby, *Maps, the Plasticity and Creep of Metals and Ceramics*, Pergamon Press, Oxford, 1982
23. H.J. Frost and M.F. Ashby, *Deformation Mechanism Maps: The Plasticity and Creep of Metals and Ceramics*, Pergamon Press, Oxford, 1982
24. E. Robinson, Effect of Temperature Variation on the Long-Time Rupture Strength of Steels, *Trans. ASME*, 1952, **77**
25. D. Liu, D.J. Pons, and E.H. Wong, Creep-Integrated Fatigue Equation for Metals, *Int. J. Fatigue*, 2017, **98**, p 167–175
26. T. Rasiawan, *The Influence of Prior Creep Damage on the Fracture Localisation in X20 CrMoV12-1 Cross-Weld Creep Tests*, University of Cape Town, Cape Town, 2017
27. S. Salifu, D. Desai, and S. Kok, Numerical Simulation and Creep-Life Prediction of X20 Steam Piping, *Materials Today: Proceedings*, 2020. https://doi.org/10.1016/j.matpr.2020.05.125
28. Pyrogel-XTE-Datasheet, High-Performance Aerogel Insulation for Industrial and Commercial Applications. https://de.aerogel.com/_reso

urces/common/userfiles/file/Data%20Sheets/Pyrogel-XTE-Datasheet.pdf
29. S. Salifu, D. Desai, S. Kok, and O. Ogunbiyi, Thermo-Mechanical Stress Simulation of Unconstrained Region of Straight X20 Steam Pipe, *Procedia Manuf.*, 2019, **35**, p 1330–1336
30. M.P.D. Matweb, X20Cr13 Stainless Steel for Medical Instruments. 2019 2019 [cited 2019 17/09/2019]. http://www.matweb.com/search/datasheet_print.aspx?matguid=81346c1935fc4e03bf5e1ee21d20c218
31. S. Salifu, D. Desai, and S. Kok, Numerical Investigation of Creep-Fatigue Interaction of Straight P91 Steam Pipe Subjected to Start-up and Shutdown Cycles, *Materials Today: Proceedings*, 2020. https://doi.org/10.1016/j.matpr.2020.05.613
32. S. Salifu, D. Desai, F. Fameso, O. Ogunbiyi, S. Jeje, and A. Rominiyi, Thermo-Mechanical Analysis of Bolted X20 Steam Pipe-Flange Assembly, *Materials Today: Proceedings*, 2020. https://doi.org/10.1016/j.matpr.2020.04.882
33. S. Salifu, D. Desai, and S. Kok, Creep–Fatigue Interaction of P91 Steam Piping Subjected to Typical Start-up and Shutdown Cycles, *J. Fail. Anal. Prevent.*, 2020, **20**, p 1055–1064
34. Dassault Simulia Systemes, *ABAQUS 6.13 User's manual.* (Providence, RI, 2013)
35. Dassault Simulia Systemes, *fe-safe/TURBOlife User Manual.* (Providence, RI, 2017), p. 122